Journal of Applied Geophysics 204 (2022) 104723

Contents lists available at ScienceDirect

Journal of Applied Geophysics

journal homepage: www.elsevier.com/locate/jappgeo

# Characteristics and rippability conditions of near-surface lithologic units (Penang Island, Malaysia) derived from multimethod geotomographic models and geostatistics

Adedibu Sunny Akingboye [a,b,*], Andy Anderson Bery [a,**]

[a] School of Physics, Universiti Sains Malaysia, 11800 Penang, Malaysia
[b] Department of Earth Sciences, Adekunle Ajasin University, 001 Akungba-Akoko, Ondo State, Nigeria

ARTICLE INFO

*Keywords:*
Multi-geotomographic modeling
Regression analysis
Rock mass quality (RMQ)
Rock quality designation (RQD)
Sustainable groundwater
Infrastructure design

ABSTRACT

The nature and rippability conditions (rock mass quality [RMQ]) of the near-surface lithologic units of Batu Maung, Penang Island, Malaysia, were investigated to develop sustainable groundwater and infrastructure. This study used a novel approach that combined seismic refraction tomography (SRT), electrical resistivity tomography (ERT), borehole drilling, and simple linear regression (SLR) analysis. The seismic P-wave velocity (Vp) and resistivity models revealed four distinctive units: residual soils (silty sand), very poor-to-good (weathered) granite, and the fresh granitic unit, including the fractured/faulted zones. The thicknesses of the residual and weathered materials ranged from a few centimeters to 15 m and 1.0–16 m, respectively. The developed empirical relationship effectively predicted rock quality designation (RQD) from Vp data through SLR analysis, with a prediction accuracy of 96% and a $p$-value$<0.05$. Also, the results from five key regression assumptions: linear relationship, multivariate normality, no multicollinearity, no autocorrelation, and homoscedasticity, suggested an accurate and statistically significant empirical relationship for use in granitic environments. The RMQ statistical model accurately classified the lithologic units beneath the area into Classes I–VI. Due to the low load-bearing of the rippable residual soils, very poor-to-fair weathered granitic rock masses, and fractured/faulted zones based on their Vp and resistivity values, and the steep slopes in the northern section of the study area, all intended infrastructures, particularly high-rise buildings and buildings with continuous footing foundations, should be piled to rest on the non-rippable fresh granitic units, with RQD and Vp values of >90% and >2100 m/s, respectively, in the central to the northcentral section in the study area. Conversely, the deep-weathered/fractured zones of depths >35 m, beneath Line 1, towards the central part of the area, with resistivity and Vp values of 100–900 Ω-m and <1900 m/s, respectively, were identified as potentially water-containing zones for sustainable groundwater abstraction.

## 1. Introduction

Rippability is a measure of how easily (or how difficultly) soils or rock masses can be mechanically excavated, such as breaking, cutting, core drilling, digging, and ripping (MacGregor et al., 1994; Basarir, 2002; Caterpillar Incorporation, 2010; Khamehchiyan et al., 2014; Jug et al., 2020). The rippability conditions of subsurface lithologic units are controlled by several factors that are attributed to the petrophysical and geomechanical properties of the formation under investigation. Generally, deeply weathered, highly stratified, fissile, laminated rocks with extensive fractures are rippable. However, fresh crystalline rocks are non-rippable (Anon, 1987, 1988; MacGregor et al., 1994; El-Naqa, 1996; Hoek and Diederichs, 2006; Basarir, 2002; Basarir et al., 2008; King, 2009; Tsiambaos and Saroglou, 2010; Griffith and King, 2011; Bery and Saad, 2012a; Liang et al., 2017; Jug et al., 2020). The rock mass quality (RMQ) of subsurface rock units is determined by their rippability strengths, which are attributed to petrophysical and geomechanical properties (Griffith and King, 2011; Jug et al., 2020). These properties are significant in any earthwork, especially highway construction and other preliminary civil engineering works, e.g., surface and underground mines, tunnel construction, and foundations (El-Naqa, 1996; Tsiambaos and Saroglou, 2010; Alavi and Sadrossadat, 2016; Shahbazi

* Corresponding author at: Department of Earth Sciences, Adekunle Ajasin University, 001 Akungba-Akoko, Ondo State, Nigeria.
** Corresponding author at: School of Physics, Universiti Sains Malaysia, 11800 Penang, Malaysia.
*E-mail addresses:* adedibu.akingboye@aaua.edu.ng (A.S. Akingboye), andersonbery@usm.my (A.A. Bery).

https://doi.org/10.1016/j.jappgeo.2022.104723
Received 3 July 2021; Received in revised form 30 March 2022; Accepted 6 June 2022
Available online 9 June 2022

et al., 2019; Jug et al., 2020). Foundations of such engineering works must rest conformably on stable strata or sound quality rock masses free of weak zones (fractures and shearing) and clay-rich soils to prevent failure, e.g., cracks, tilting, and even total collapse, due to ground subsidence, soil sliding, and excessive differential settlement (Ganerød et al., 2006; Akingboye and Osazuwa, 2021; Lee et al., 2021). Conversely, lithologic units with low load-bearing strengths due to weathering and fractures with good apertures and quality residual soils can serve as suitable conduits for groundwater storage (Akingboye et al., 2022).

Selecting the most appropriate excavation/rippability method is one of the most crucial tasks during the design and construction of infrastructure. This is particularly important as it will improve the prediction of the excavation effort, accelerate the turnaround time of the construction plan, facilitate the selection of proper extraction equipment, maximize the overall operation and production costs, and improve the durability of the infrastructure (Liang et al., 2017; Shahbazi et al., 2019; Jug et al., 2020). Several rippability classification systems, including direct and indirect classification systems, have been developed to assess the rippability of near-surface rock masses. The direct rippability classification system entails the direct ripping of rocks in the field with a dozer. The indirect rippability classification system, on the other hand, uses rock mass and material properties to estimate the rippability of rocks (Basarir, 2002; Basarir et al., 2008; Caterpillar Incorporation, 2010). Many researchers, so far, have developed indirect rippability classification methods and are categorized as seismic velocity-based methods, graphical methods, and grading methods (e.g., Bailey, 1975; Anon, 1987, 1988; Hoek and Brown, 1997; Hoek and Diederichs, 2006; Del Potro and Hürlimann, 2009; Caterpillar Incorporation, 2010; Liang et al., 2017; Jug et al., 2020).

Seismic velocity-based methods use seismic P-wave velocity (Vp) to estimate the rippability of rock. The obtained Vp values for subsurface rock units are usually correlated with their rippability values based on proposed charts by the Dozer companies such as Caterpillar Inc. (Anon, 1988; Caterpillar Incorporation, 2010) and Komatsu (Anon, 1987). The charts converted measured Vp models into rippability values based on a developed ripper model. The rippability models derived from such charts do not consider important factors like rock hardness, weathering, joint spacing, discontinuity, and strike and dip of the bedrock (Basarir, 2002; Caterpillar Incorporation, 2010; Khamehchiyan et al., 2014). Seismic refraction tomography (SRT) has been widely used to characterize subsurface lithologies (Sheehan et al., 2005; Quigley, 2006; Azwin et al., 2013; Bery, 2013; Ronczka et al., 2018; Lee et al., 2021), and to indirectly determine the degree of rippability of rock masses (Hoek and Brown, 1997; Tsiambaos and Saroglou, 2010; McCann and Fenning, 2015; Ismail et al., 2017; Shahbazi et al., 2019; Jug et al., 2020). Masked layers, hidden layers, and water infills are some of the drawbacks that can prevent accurate delineation of lithological characteristics using the SRT technique (Bery and Saad, 2012a; Akingboye and Ogunyele, 2019; Hasan et al., 2021). Additional rock properties and filtering processing can help to solve these problems. In addition, the use of borehole logs could accurately constrain the SRT model, providing more details on actual subsurface lithologies and addressing the drawbacks.

Conventionally, researchers mainly use seismic refraction and borehole (rock core sample) methods to evaluate RMQ based on rock quality designation (RQD). However, electrical resistivity tomography (ERT) has a wide range of resistivity values, offers a strong link between resistivity and subsurface lithology, and provides the requisite depths of probing compared to other geophysical methods (Akingboye and Ogunyele, 2019; Hung et al., 2020; Hasan et al., 2021; Akingboye and Bery, 2021a, 2021b, 2022; Akingboye et al., 2022). As a result, it is envisaged that ERT combined with SRT and borehole logs will provide more details on subsurface litho-structural conditions of the area under study.

The present study was carried out in the southern part of Penang Island, Malaysia. Penang Island is Malaysia's second-most developed state, with the second-largest population. The landmass of Penang Island is small and has resulted in an increasing number of high-rise buildings over the years. Regardless of the number of buildings in the area, the growing population of residents and tourists on Penang Island necessitates the development of more durable infrastructure and sustainable potable water. Since high-rise buildings are built more frequently in this area, detailed characterization of the near-surface geology is essential for their construction and sustainable potable groundwater development. Previous studies on rock rippability assessment in Malaysia, for example, Mohamad et al. (2005), Ismail et al. (2017), Hazreek et al. (2018), Tawaf et al. (2018), used seismic refraction and borehole methods. Still, only a few pieces of information on the rippability of near-surface rock masses of the granitic terrain of Penang have been provided. Therefore, we used a novel approach that combines SRT, ERT, borehole drilling, and simple linear regression (SLR) analysis to evaluate the nature and RMQ of near-surface lithologies at Batu Maung, Penang Island, Malaysia, for the construction of residential buildings and potable groundwater development. Holistically, it is expected that the methodologies used will yield more precise results than the combined use of SRT and borehole data. As a result, the developed empirical relationship between RQD and Vp and the overall findings of this study will significantly contribute to the characterization of near-surface geology and RMQ in granitic environments.

## 2. Methods

### 2.1. Geological setting of the study area

The studied site is located within Batu Maung, Penang Island, Malaysia (Fig. 1). Penang Island is located in the Malacca Strait, northwest of Peninsular Malaysia, and is underlain by the Gula, Beruas, and Simpang Formations (Hassan, 1990). The main section of Penang Island is underlain by igneous rock, typically granite (Fig. 1a and b), which was emplaced as other Malaysian granitoids. The Malaysian granitoids (Fig. 1a) constituting the Eastern Belt Indo-China domain and the Western and Central Belts of the Sibumasu domain are typically Permian to Late Triassic I-type granites and Late Triassic S-type granites, respectively (Ng et al., 2015). The Western and Central Belts of the Sibumasu domain are typically biotite granites and granodiorites, respectively (Ng et al., 2015). The S-type granites of the Western and Central Belts and the I-type granites of the Eastern Belt were primarily formed by the partial melting of the metamorphic basement of the Sibumasu Block and the Indo-China Block, respectively, as a result of their collision (Ng et al., 2015; Cao et al., 2020). This collision event also resulted in the formation of the predominant approximately NS trending faults in the area (Abdullah and Purwantoa, 2001; Ng et al., 2015; Cao et al., 2020).

The granites of Penang Island (Fig. 1b) are primarily composed of two Plutons, namely the North Penang Pluton and the South Penang Pluton, and were classified based on the proportion of alkali to total feldspar content (Ong, 1993). Tanjung Bungah, Paya Terubong, Batu Ferringhi groups, and the Muka Head micro granite are the North Penang Pluton type granites and are orthoclase to intermediate microcline feldspar-rich. The medium to coarse-grained biotite granites of Tanjung Bungah were formed in the Early Jurassic. The Paya Terubong group, ranging in age from the Early Permian to the Late Carboniferous, is distinguished by medium to coarse-grained biotite granites with microclines. The Batu Ferringhi group, consisting of medium to coarse-grained biotite granites with predominantly orthoclase to intermediate microcline feldspar, is located on the northwestern coast of Penang Island and was formed in the Early Jurassic age. Microcline feldspar granites, including the Batu Maung granites, are found in the South Penang Pluton (Ong, 1993; Ahmad et al., 2006).

### 2.2. SRT field data acquisition and inversion processing

The study area is located in an undeveloped area of Batu Maung,

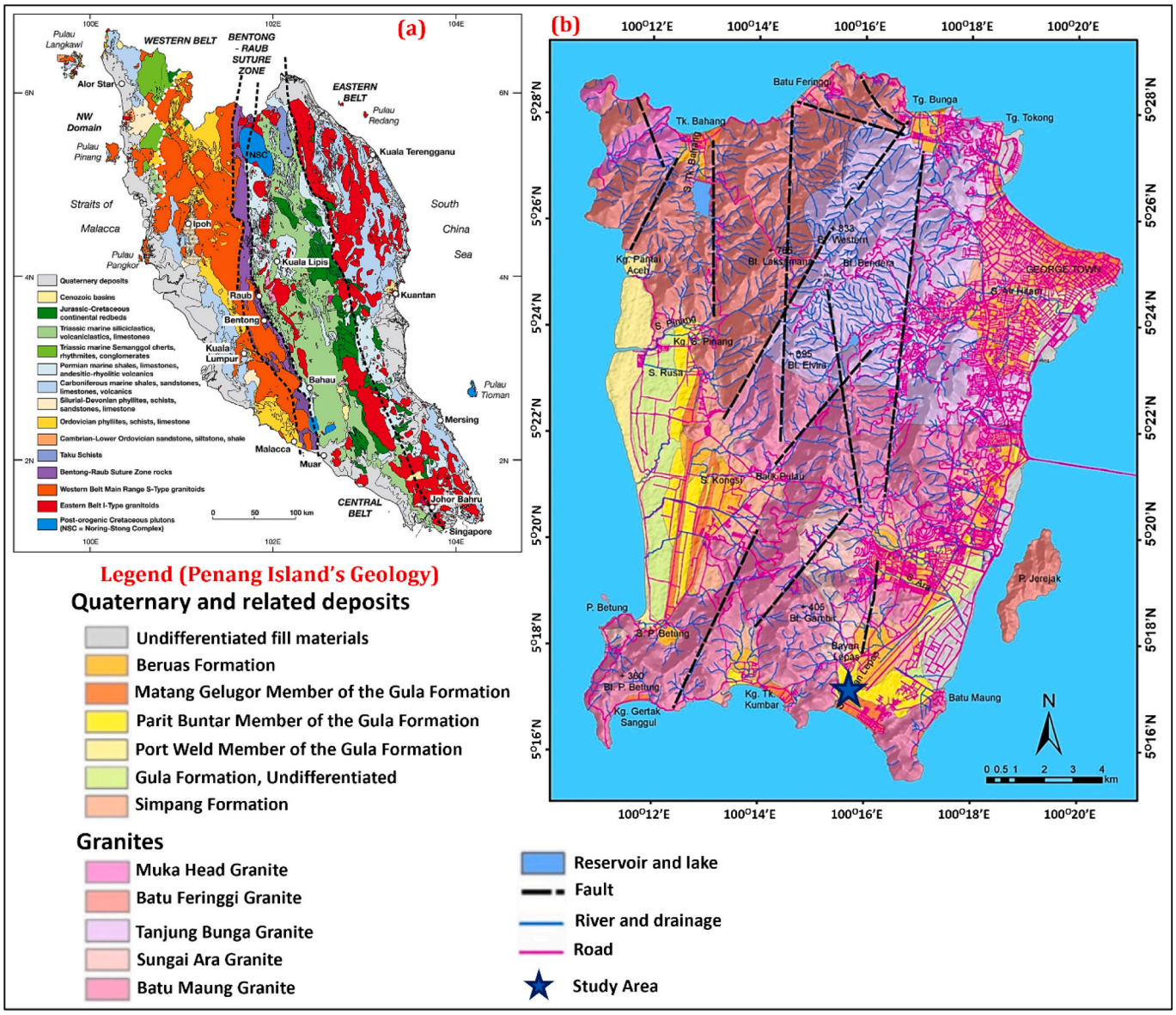


**Fig. 1.** (a) Simplified regional geological map of Peninsular Malaysia (after Tate et al., 2009) (b) Detailed geological map of Penang Island, Malaysia (modified after Ahmad et al., 2006; Abdul Hamid et al., 2019).

Penang Island, Malaysia (Fig. 2a), along the major road to Penang Airport. The geophysical investigations used SRT, ERT, and borehole techniques (Fig. 2b–g) to characterize and determine the rippability conditions of the subsurface lithologic units for the construction of residential buildings and groundwater development in the study area. Four seismic lines were established in the study area. Lines 1 and 2 and Lines 3 and 4 were oriented roughly NW-SE and NE-SW, respectively (Fig. 2a). Three lines covered a total distance of 115 m each, using a 5 m geophone interval, except for Line 1, which had an 80.5 m traverse length and a 3.5 m geophone interval. Six boreholes (BH1 to BH6) were drilled in the surveyed site (Fig. 2a and g). Some stations on the lines share the same boreholes due to stations' coincident or closeness to the boreholes.

The seismic velocity measurements were acquired using the ABEM Terraloc Mark 8 instrument. The SRT technique recorded the seismic velocities of the near-surface lithologic units beneath the study area via non-destructive probing seismic waves from shot points through a striker metal plate, 12-pound hammer, and a channel of 24 geophones at 14 Hz (Fig. 2b). More clustered shot points were used at the offsets because of the distance between the shot point and the geophones (Fig. 2c). The goal was to create a velocity model with a high signal-to-noise ratio and deeper depth resolution. For each SRT line, about 360 seismic traces were recorded from 15 shot points. As shown in Fig. 2d, SRT measures the traveltimes of compressional seismic waves (or P-waves) that were refracted at the interfaces between subsurface layers of varying velocities. However, some generated waves (regarded as noise) are usually present alongside measured P-waves. The seismograph automatically summed the seismic responses received during field measurements, canceling extraneous impulses (i.e., noise). The rest of the noise was removed during field data reduction and processing (Quigley, 2006; Akingboye and Ogunyele, 2019).

The obtained field seismic data sets were processed using the SeisOpt@2D software. SeisOpt, unlike other seismic software, avoids the ray-tracing method in favor of nonlinear optimization (i.e., generalized simulated annealing method) to invert the first arrival traveltimes (Quigley, 2006; Akingboye and Ogunyele, 2019). Traveltime inversion using linearized inversion techniques does not typically account for changes in ray path velocities, making it initial velocity model-

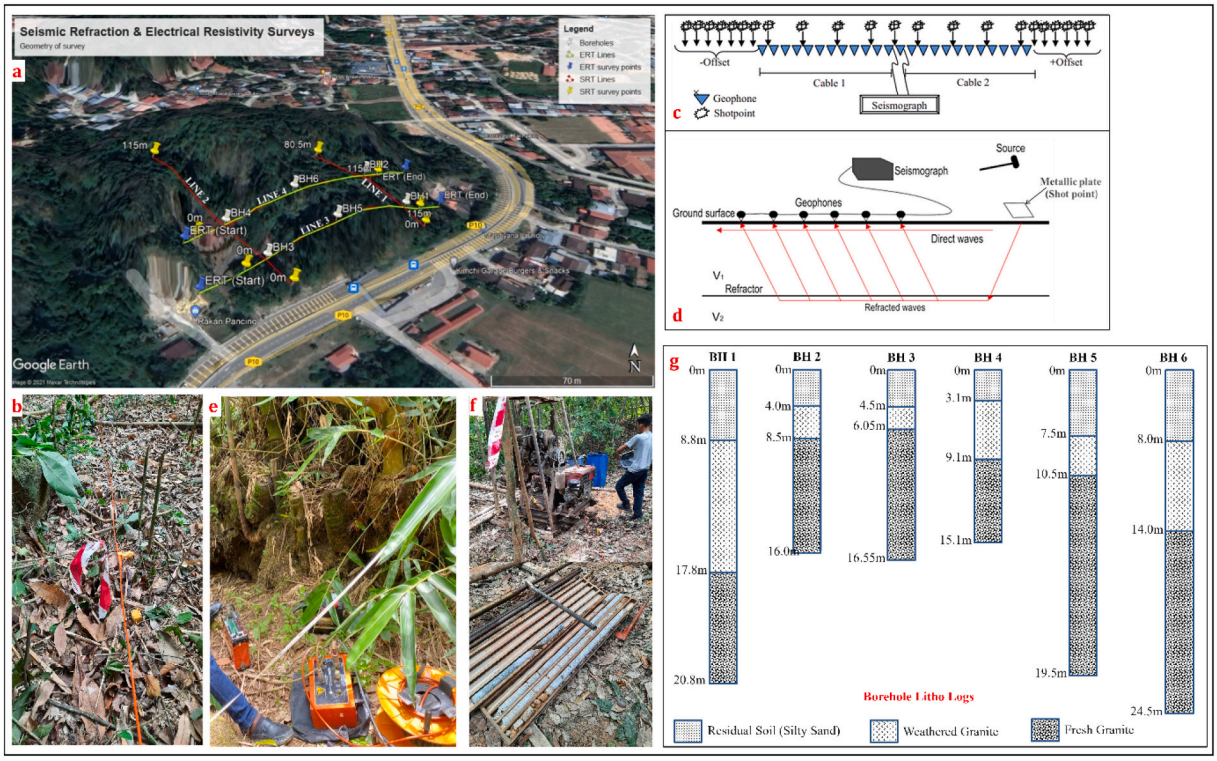


**Fig. 2.** (a) Aerial data acquisition map of the study area showing the occupied SRT and ERT geophysical lines and borehole (BH) locations. (b) SRT data acquisition setup showing the geophones' cable connected to a grounded geophone. (c) A typical SRT data acquisition layout displaying an array of geophones, geophones' cables connected to a seismograph, and location of shot points. (d) The progression of seismic P-waves generated at the surface refracted at boundary surfaces for a typical two-layer model. (e) Image of ERT measuring units used for the ERT data acquisition. (f) Image of the core drilling machine and the recovered core samples showing their lengths and sizes. (g) Litho logs of BH1–BH6 in the study area.

dependent and potentially resulting in incorrect solution convergence. Most importantly, SeisOpt's forward modeling uses a fast finite-difference method based on a solution to the eikonal equation to compute first arrival traveltimes (e.g., Pullammanappallil and Louie, 1994; Quigley, 2006; Akingboye and Ogunyele, 2019). Furthermore, FirstPix was used to select and manually edit the first-time arrivals (P-waves) from the gamut of gathered seismic waves. The low and weak Vp responses arising from thin or low-velocity layers beneath thick and high-velocity layers were enhanced via the automatic gain control technique for detailed mapping of the hidden zones. After that, the refraction inversion optimization technique was used to invert all the picked first arrival times in high-resolution mode. Hence, the resulting subsurface velocity model was generated after completing the number of predefined iterations (Fig. 3a). The final Vp models of the study area were remodeled using Surfer software to produce subsurface Vp geotomographic and geological/rippability models, depicting the nature and rippability conditions of near-surface geology. The Vp, which measures the depth of propagation and traveltimes, depends on the compactness and thickness of the subsurface lithologic unit through which it propagates, as presented in the rippability chart proposed by Caterpillar Incorporation (2010), Fig. 3b.

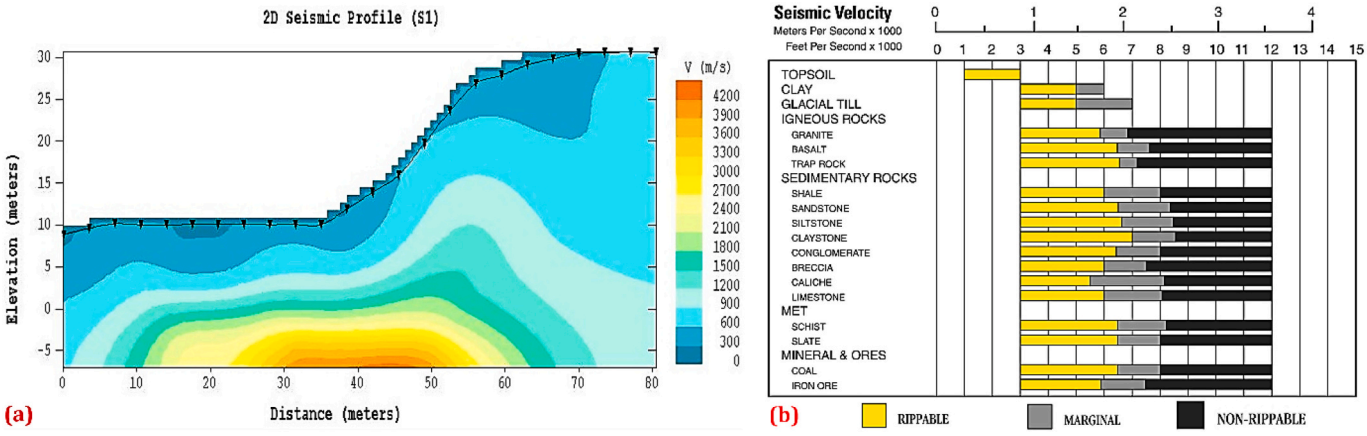


**Fig. 3.** (a) Final inverted SRT model produced from the SeisOpt@2D software for Line 1 in the study area. (b) A typical rippability prediction chart based on seismic velocity values, showing the ripper performance for Caterpillar D8R/D8T Rippers and the relationships between seismic velocities and crustal materials (modified from Caterpillar Incorporation, 2010).

### 2.3. ERT field data acquisition and inversion processing

ERT is a non-invasive geophysical technique that is versatile enough in characterizing and resolving complex subsurface geology (Binley and Kemna, 2005; Bery and Saad, 2012a, 2012b; Cheng et al., 2019; Akingboye and Osazuwa, 2021; Akingboye and Bery, 2021a, 2021b). In the study area, only two lines were investigated for ERT measurements due to the ruggedness and steepness of the hilly sections along Lines 1 and 2, making it very difficult to spread out ERT cables and grounding electrodes. Lines 3 and 4 were investigated using a 4.0 m electrode spacing over a profile length of 160 m each (see Fig. 2a). ERT Lines 3 and 4 were established 38 m and 11 m away from the first borehole locations on each line, respectively, because the ERT lines were longer than those of the SRT. This ensured that the positive 5 m station positions on the ERT lines coincided with the 5 m station positions on their SRT lines for the borehole locations to be consistent. The purpose of the ERT survey was to provide additional subsurface clues to accurately infer the conditions of the near-surface lithologies and structural dynamics of the area.

The resistivity values were measured using the Lund Imaging Resistivity Meter (a combination of the ABEM SAS Terrameter 4000 and the ES 64–10C Electrode Selector with their accessories), Fig. 2e, with the Wenner-Schlumberger array type. The Wenner-Schlumberger array can probe to a greater depth and is moderately sensitive to horizontal and vertical structures. As a result, it can optimize the signal-to-noise ratio to produce a high-resolution inverse resistivity model with minimal or zero distorted structural artifacts (Loke, 2004; Loke et al., 2013; Akingboye and Ogunyele, 2019; Akingboye and Bery, 2021a, 2021b). The quality of the resistivity data was enhanced by applying stacking processes to increase signal strength. The apparent resistivity measured in the field assumes that subsurface lithologies are homogeneous. Thus, the apparent resistivity data must be inverted to obtain the true resistivity values of the subsurface lithologic units.

The acquired resistivity datasets with topography were processed and inverted using the RES2DINV software, following the least-squares inversion procedures described in the works of Akingboye and Bery (2021a, 2021b, 2022). The employed finite-element method of four nodes with $L_2$-norm as the standard least-squares constraint parameter minimized the difference between the measured and calculated apparent resistivity values. A damping factor of 0.05, with a minimum value of 0.01, was used to improve the accuracy and resolution of the calculated and observed apparent resistivity model. The inverse model convergence (root mean square) error was below 10% for a maximum of 5 iterations. The generated composite sections, consisting of the measured and calculated pseudosections and the two-dimensional (2D) inverted resistivity sections beneath the ERT Lines 3 and 4, are shown in Figs. 4 and 5. The resistivity models were interpreted based on borehole data as geologic references like the velocity models.

### 2.4. Borehole drilling and rock mass rippability and quality modeling

To obtain precise information about the nature of near-surface granitic rock masses in the study area, a Caterpillar Field Core Drilling Machine, as shown in Fig. 2f, was used to drill the topsoil until fresh competent bedrock was encountered, and cored samples were recovered from the drilled six boreholes (BH1–BH6). The recovered in situ cored samples from the boreholes were arranged in the core sample boxes, one for each borehole (see Fig. 2f). The borehole logs (Fig. 2g) were integrated with the observed Vp and resistivity models for accurate delineation of lithologies with their respective depths, and primarily for determining the RQD to evaluate the RMQ of the rock masses beneath the surveyed site.

### 2.5. Rock quality designation (RQD) analysis and modeling of RMQ

RQD is a common parameter for evaluating the quality of rock masses. The information derived from this parameter is critical for determining foundation depth, the bearing-load capacity of rock masses, differential settlement, and foundation sliding possibility (Deere, 1989; Barton et al., 1974; Hoek and Brown, 1997; Hoek and Diederichs, 2006; Griffith and King, 2011). In order to determine the nature and rippability/RMQ of the underlying rock masses based on their RQD values, forty-five recovered core samples (core sample numbers, $n = 45$) from BH1–BH6 in the surveyed site were used. RQD values of rock masses beneath the surveyed site were estimated using Eq. 1, suggested by Abzalov (2016). The derived RQD values were cross-checked against 2D Vp models at the same depths for their corresponding velocities. Through this, insights were adequately gathered about weathering, fracture density, load-bearing strength of the near-surface rock masses, and the groundwater condition of the study area. At the time drillings were carried out, the water table in the study area varied between 2 m and 5 m, depending on the thickness of the residual soils.

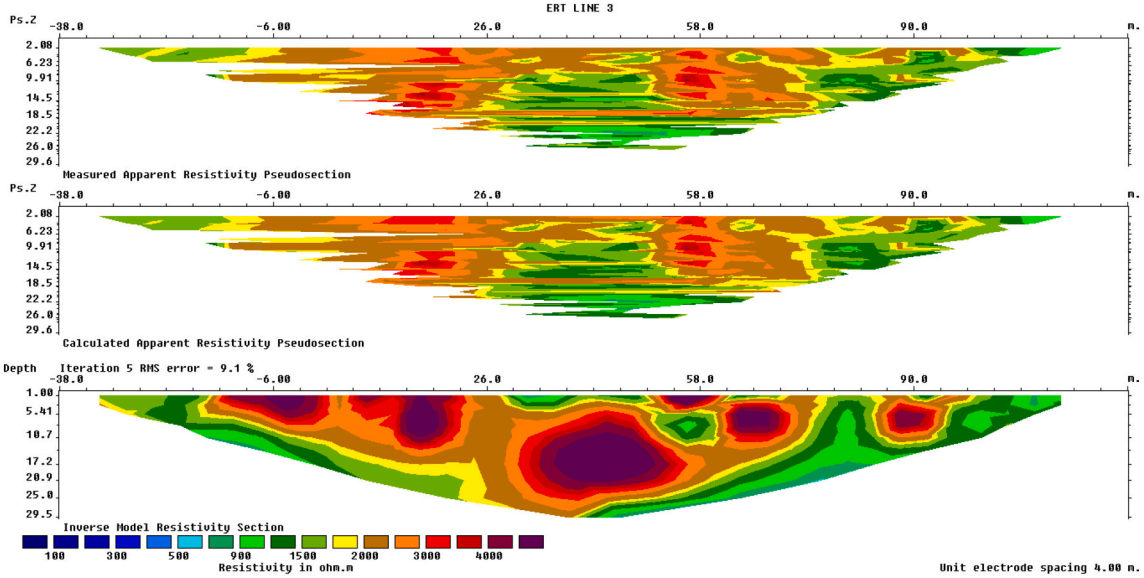


**Fig. 4.** Composite results of the 2D ERT inversion beneath Line 3.

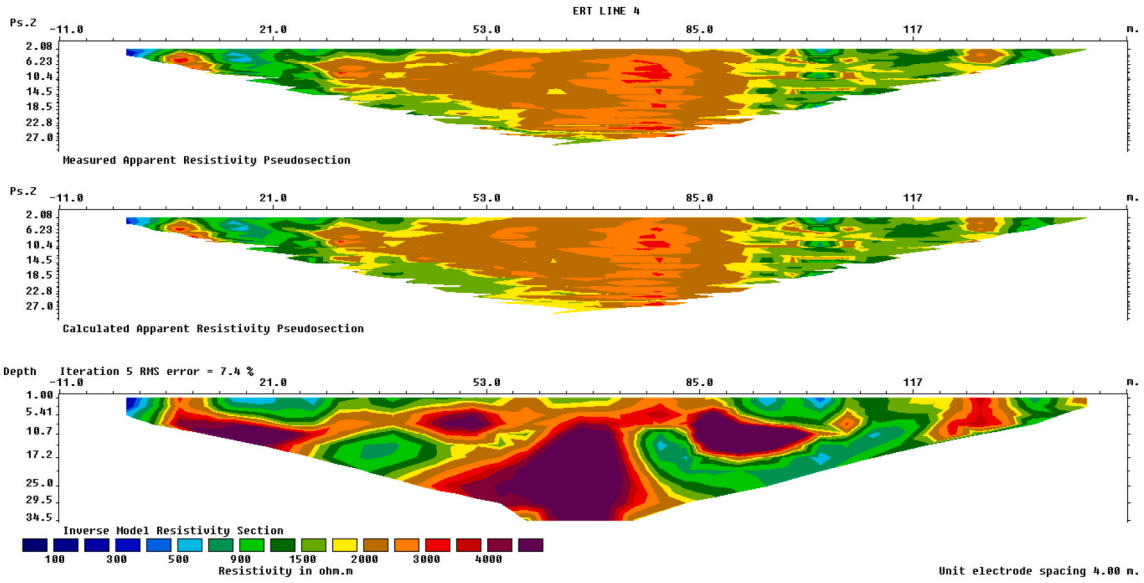


**Fig. 5.** Composite results of the 2D ERT inversion beneath Line 4.

$$RQD\ Index\ (\%) = \frac{\sum length\ of\ sound\ pieces > 100\ mm\ (4\ in.)}{Total\ core\ run\ length} \times 100 \qquad (1)$$

As a new data set for statistical model analysis, the RQD values for the subsurface rock masses beneath the research region were plotted against their corresponding Vp values (based on the same depth and distance) to generate the RMQ plot. The accuracy of the statistical model was evaluated using the IBM SPSS (v26) software to evaluate correlation coefficient (R), Durbin-Watson (D-W), multivariate normality, multicollinearity (i.e., tolerance and variance inflation factor, VIF), analysis of variance (ANOVA), and homoscedasticity of the used variables (RQD and Vp data). The RQD and Vp values were respectively regressed as dependent and independent variables to confirm the empirical relationship between both used parameters and accurately predict the RMQ of the near-surface rock masses in the study area.

## 3. Results

### 3.1. Interpretation of the study area's seismic velocity and rippability models

The 2D inverted velocity and the rippability models of the near-surface for the four seismic refraction lines in the study area are shown in Fig. 6a–h. Fig. 6a–d depicts the seismic velocity models of the near-surface lithologic units beneath Lines 1–4. Four distinct layers, namely the residual soils (silty sand in nature), weathered (very poor-to-good) granitic units, and fresh granitic bedrock, including the fractured/faulted bedrock, were delineated beneath the study area. Table 1 shows that the minimum and maximum Vp values varied between 200 m/s and 4200 m/s for the identified lithological units beneath the studied site. The first layer, constituting the residual soils at the near-surface depth, had seismic velocity values of 200–800 m/s. The second layer (very poor-to-good granite) had velocity values ranging between 800 m/s and 2000 m/s. Lastly, the third layer (fresh granitic bedrock) depicted velocity values of >2000 m/s. However, fractures (F) were mapped beneath the study area. The 2D rippability models (Fig. 6e–h) show the interfaces of the three layers based on the range of velocity values. The residual soils were interpreted as the rippable layer. The very poor-to-good weathered granitic units were identified as the marginal unit, occurring between the rippable and the non-rippable layer (fresh granitic bedrock), with Vp values above 2000 m/s. The interpretations were based on the borehole-derived litho logs and the rippability chart proposed by Caterpillar Incorporation (2010), Fig. 3b.

In Fig. 6a and e (seismic velocity and rippability models of Line 1), the thickness values of the rippable residual soils ranged between 8 m and 17 m. This layer slopes gently from the southeastern part with the thickest soil profile to the northwestern section of the area, with a pronounced steep slope between station distances of 38 m and 58 m. The very poor-to-good granitic units had thickness values ranging from 6 to 12 m. Due to fracture (F2), the layer bulged upward with a curved base between station distances of 45 m and 70 m. Also, the high erodibility of the steep sections might be responsible for the thinning of the weathered layer in the southeastern area, resulting in a low-load sediment pile. Similarly, in Line 2 (Fig. 6b and f), the three lithologic units had almost the same velocity trends and subsurface features, including steep topography, as identified beneath Line 1, since both lines are parallel to each other. However, the first two layers beneath Line 2 are thinner than those delineated beneath Line 1, and the non-rippable granitic unit outcrops massively at the near-surface. The rippable residual soil was 1–12 m thick. The thicknesses of the weathered marginal units ranged from 5 to 15 m. The deepest sections were characterized by fractures (F3 and F4), responsible for the partial to deep weathering of the granitic bedrock. Most importantly, the observed variations in the thicknesses of lithologies beneath Lines 1 and 2 indicate sediment thickening towards the eastern part of the study area, arising from high weathering rates and accumulation of eroded soils from the northwestern section.

As seen in Line 3 (Fig. 6c and g), the Vp model shows that the ground topography is primarily flat, with a few minor kinks. The thicknesses of the rippable residual soil and the weathered marginal units ranged from <1 m to 11 m and 6 m to 18 m, respectively. Two oppositely inclined fractures (F5 and F6) were mapped between station distances of 10 m and 30 and 60 m and 70 m, respectively. The non-rippable granitic unit is considerably deeper than its northward position beneath Line 4 (Fig. 6d and h). As shown in Fig. 6d and h, Line 4 had steeper surface topography, shallower residual soil, and weathered granite than Line 3. F7 and F8 were delineated between station distances of 65 m and 100 m beneath Line 4. The comparison of Lines 3 and 4 tomographic models indicates that the outcropping non-rippable granitic unit increases northward. Similarly, the weathered soil profile's thickness increased eastward and towards the western end of the study area.

### 3.2. Interpretation of the resistivity models derived for the study area

The resistivity models beneath Lines 3 and 4 (Fig. 7a–b) depict

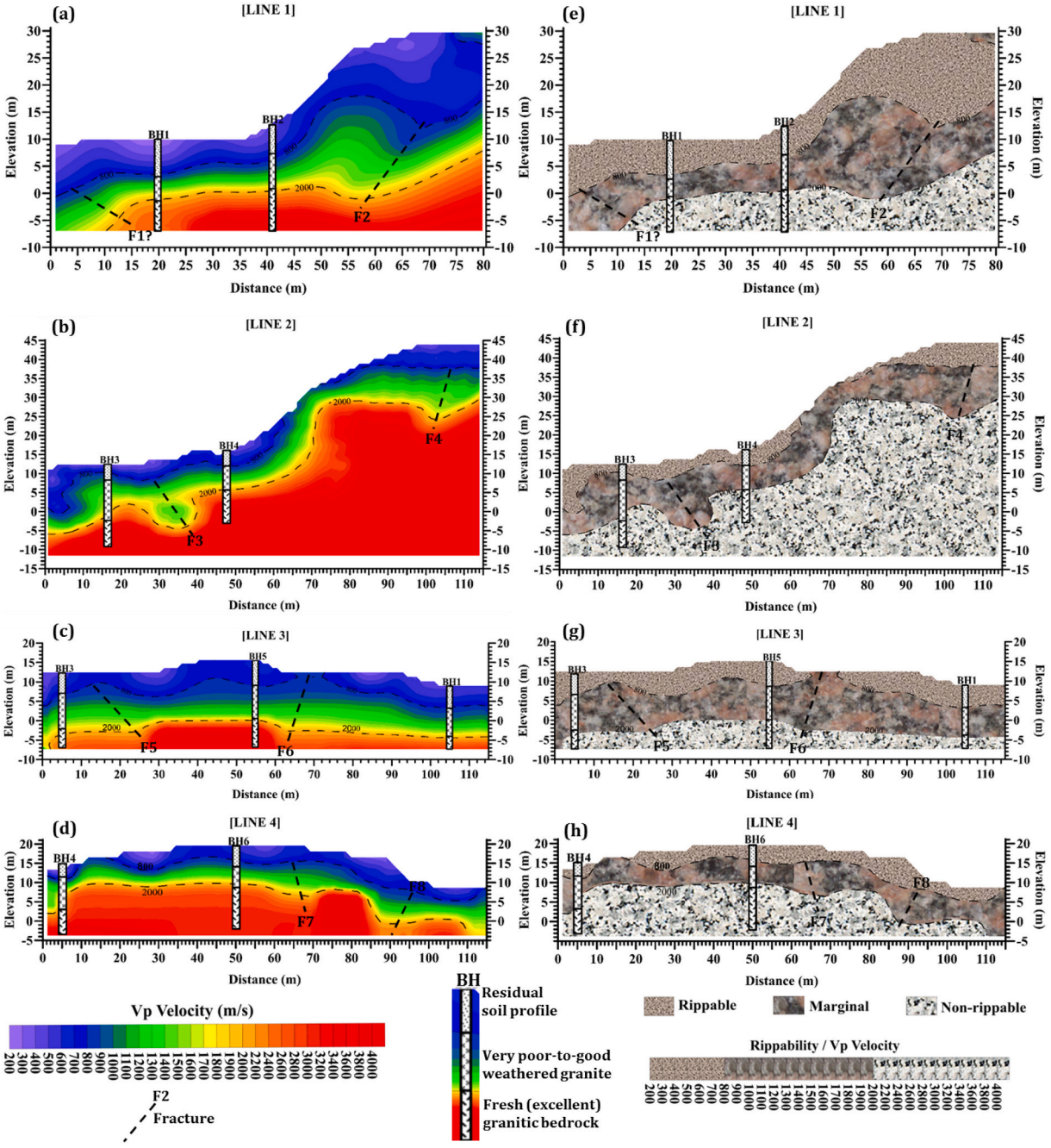


**Fig. 6.** Images a–d show the 2D inverted seismic refraction geotomographic models, whereas images e–h represent the subsurface geological models showing the rippability conditions of the near-surface lithologic units beneath Lines 1–4. *F denotes fractures, and BH stands for the drilled boreholes in the study area.*

**Table 1**
A comprehensive summary of the observed seismic velocity interpretation in relation to borehole litho-sections for the investigated traverse lines in the study area.

| Lines | Near-surface lithologic units (soil/rock) | Seismic velocity, $V_p$ (m/s) |
|---|---|---|
| All seismic velocity models | Residual soils | 200 to <800 |
| | Very poor-to-good (weathered) granite | 800–2000 |
| | Fresh granitic unit | >2000–4200 |

corresponding subsurface characteristic features with their SRT models at nearly the same station positions. The range of resistivity values for residual soil, very poor-to-good granitic bedrock, and fresh granitic units conformed with the borehole-derived litho logs. High resistivity values indicate bedrock or boulders (outcropping at the surface or near-surface depths) and stiff-to-hard silty sand and/or sand. The silty sand topsoil across the surveyed site was thin, with resistivity values ranging from 100 to >1000 Ω-m. The resistivity values of the poor-to-good granitic units varied between 900 Ω-m and 2000 Ω-m, whereas the fresh granitic unit exceeded 2000 Ω-m. The observed high resistivity values for the top layer and weathered granitic units were attributed to the nature and compactness of the silty sand. The granitic bedrock beneath the surveyed site was characterized by deep-weathered/fractured zones. In addition to the fractures identified in the velocity models, more penetrative fractures were delineated beneath Lines 3 and 4 in Fig. 7a–b. Some of these fractures, especially F6, F7, and F8 in Fig. 6, conformed with those delineated as F11, F16, and F18 on the ERT models (Fig. 7).

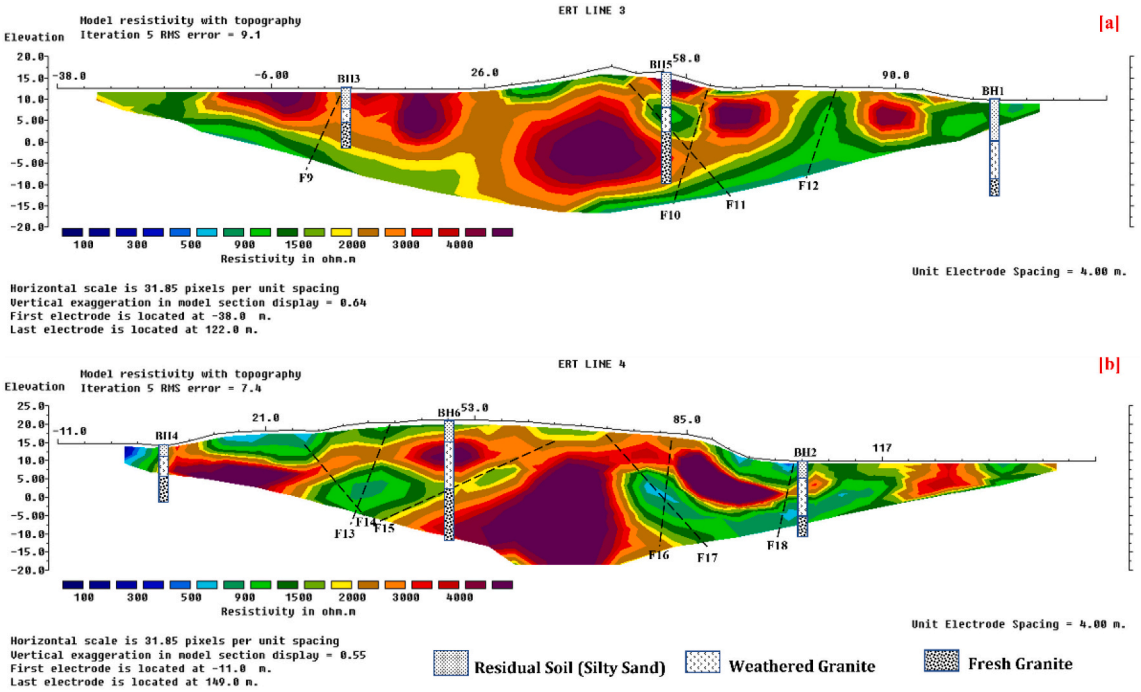


**Fig. 7.** Inverse model resistivity sections beneath Line 3 (a) and Line 4 (b), respectively, in the study area. Negative distance implies the coverage area is located on the left side of 0 m of SRT traverses.

The resistivity models clearly show the weathering of the granitic bedrock to depths >20 m, arising from seepages and groundwater stored within the deep-weathered zones. The velocity models could not image the deeply weathered profiles underlying the fresh bedrock. However, the central bedrock is stable, depicting the highest resistivity values.

## 4. Discussion

### *4.1. Characterization of the seismic velocity, georesistivity, and rippability conditions of the near-surface lithologic units*

Subsurface Vp and resistivity values ranging from 200 to 4200 m/s (Fig. 6a–h) and 100–5000 Ω-m (Fig. 7a–b) mirrored the nature, thicknesses, and structural conditions of the delineated near-surface geology in the study area. The Vp and resistivity values in the study area varied due to the petrophysical and geomechanical properties of the subsurface geology. These include properties such as uniaxial strength, compactness, abrasiveness, density/hardness, porosity, permeability, degree of void ratio, degree and depths of weak zones (weathered troughs, fractures/faults, and sheared zones), etc., (Hoek and Diederichs, 2006; Caterpillar Incorporation, 2010; Griffith and King, 2011; Bery and Saad, 2012a; Liang et al., 2017; González et al., 2019; Jug et al., 2020; Akingboye and Bery, 2021a, 2021b, 2022).

Fig. 8a–b shows the 3D seismic Vp geotomographic model and the rock mass rippability model of the lithologic units beneath the study area. The near-surface lithologic units of the study area were classified

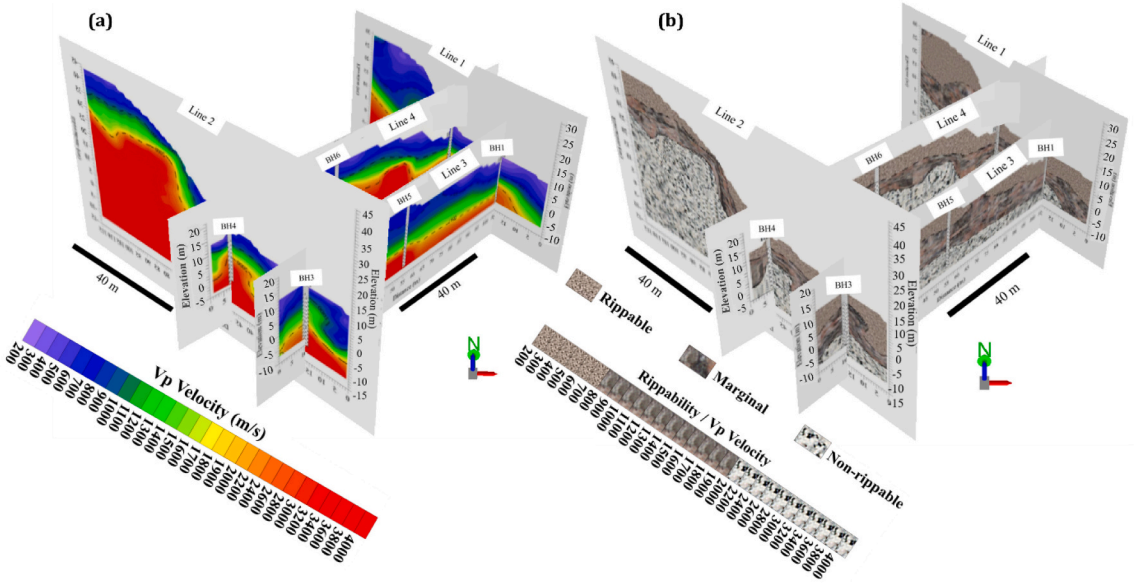


**Fig. 8.** (a) 3D seismic Vp geotomographic model and (b) 3D rock mass rippability model of the near-surface lithological units in the study area.

as rippable residual soils, and very poor-to-good granitic units, and non-rippable fresh granitic units, with varied Vp values of about 200 to <800 m/s, 800–2000 m/s, and >2000 m/s, respectively. Interestingly, Fig. 8a–b depicts the rippable overburden materials with thick residual soil profiles towards the eastern and northeastern flanks of the surveyed site. The thicknesses of the very poor-to-good granitic units were uniform, except for sections with fractures (F1–F8) and the weathered troughs at the northeastern, eastern, and western ends of the study area. The non-rippable granitic unit, on the other hand, plunges from the north towards the southern section of the study area. Given the evidence of the surface topography of the upland sections in the study area, as shown beneath Lines 1 and 2 (Fig. 6e–f), the erodibility of the residual soils was significantly increased, allowing sediment piles of appreciable thickness to be deposited at the base of the steep slopes, as seen beneath Lines 3 and 4. The Vp models (Figs. 6 and 8) and resistivity models (Fig. 7a–b) show multiple penetrative fractures (F1–F18) in various axial directions. The identified structures had contributed significantly to the low load-bearing capacity of the near-surface; hence, detrimental to infrastructure. However, the delineated fractures beneath Lines 3 and 4 are significant for sustainable groundwater development in the study area.

### 4.2. *Evaluation of statistical models and empirical relationships: Insights into RQD and RMQ*

To understand the rippability conditions and RMQ of the rock masses, we determined the empirical relationship between RQD and Vp from forty-five borehole cores from the marginal and non-rippable rock masses beneath the study area. Deeply weathered rock masses which did not meet the RMQ requirements, as suggested by Deere (1989), Griffith and King (2011), and Abzalov (2016), among others, were excluded from consideration for the RQD evaluation. RQD is vital for assessing the quality of borehole cores and evaluating rock exposures in the field to provide a ready indicator of rock quality. RQD is used to assess RMQ based on the degree of fracturing, jointing, and shearing (e.g., Barton et al., 1974; Griffith and King, 2011; Abzalov, 2016). The recovered borehole cores from the surveyed site were analyzed for the RQD values of each of the samples using Eq.1, and their corresponding Vp values were also determined from the Vp models. According to Bery and Saad (2012a), Balarabe and Bery (2021), and Akingboye and Bery (2022), data from ≥31 sampled points are considered adequate for use and can give accurate results in statistical data analysis. The obtained RQD and Vp values were analyzed using Excel software to determine their trends, the empirical relationship between RQD and Vp for typical tropical granitic units, and the RMQ classes for the lithologic units in the study area.

The SLR plot of RQD against their corresponding Vp values (Fig. 9 and Table 2) classified the lithologic units beneath the study area into

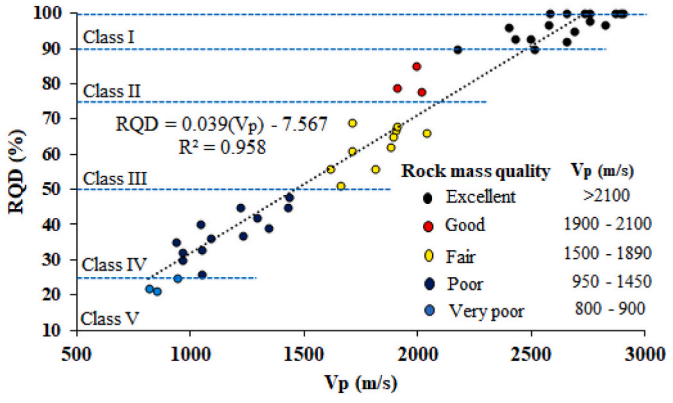


**Fig. 9.** Statistical plot of RQD against Vp for forty-five borehole core samples, ranging from very poor to excellent rock masses beneath the surveyed site.

five classes based on the derived RQD index values, as suggested by Abzalov (2016). Class V, with Vp values ranging from 800 to 940 m/s and with RQD index values of <25%, indicated very poor granitic rock masses. Vp values in Class IV ranging from 950 to 1450 m/s, with RQD index values of about 25 – 50%, indicated the poor granitic rock masses. Class III, with Vp values of 1500–1900 m/s and RQD index values of >50–75%, indicated the fair quality granitic rock masses. Class II represented the rock masses between the marginal and non-rippable granitic units. These rock masses had Vp values between 1900 m/s and 2100 m/s and RQD index values ranging from >75 – 90% and were categorized as granitic rock masses of good quality. Finally, Class I indicated the non-rippable granitic rock masses of excellent quality, with Vp values >2100 m/s and RQD index values ranging from >90 – 100%. Although Class VI, as listed in Table 2, denoting the class for the rippable residual soils, was not considered for the RQD assessment because they did not meet the RQD criteria for RMQ evaluation. But the inclusion of Class VI in the study offered additional clues in understanding the likable range of Vp and RQD values for rippable units (especially with thin layers) in tropical granitic environments. Instead of the three classifications in Fig. 8b, we were able to distinguishably classify the RMQ of the near-surface rock masses into Classes I–VI based on the SLR model (Fig. 9). Unlike other granitic rock masses with greater Vp values at depths of tens of meters or kilometers (e.g., Barton, 2007), the derived Vp values for rock masses in this study were lower due to their shallow depths. The rock masses were subjected to progressive weathering and, most likely, fracturing due to this action, diminishing their compressive and rippability strengths. As a result, the applicability and efficiency of geostatistics in assessing RMQ have been demonstrated in this study.

Empirically, the derived relationship between the RQD and Vp for the study area, as presented in Eq. 2, yielded a strong coefficient of determination value, i.e., R-squared ($R^2$), of 0.958 (Fig. 9). Hence, the result suggested a strong linear relationship between the used parameters (RQD and Vp), as Akingboye and Bery (2022) explained. A high RQD index is a function of high Vp for a rock mass to fulfil the RMQ criteria for infrastructure designs. It implies that the good and non-rippable rock masses, with RQD index values of 75–100%, are suitable for infrastructure placement (Griffith and King, 2011; Abzalov, 2016; Ismail et al., 2017; Jug et al., 2020). From the statistical plot (Fig. 9), the derived empirical relationship (Eq. 2) can, therefore, be adopted for the prediction of RMQ based on the estimation of the RQD of near-surface lithologic units from their measured Vp values for other locations in the study area and other tropical granitic environments with the same characteristic features.

$$RQD\ (\%) = 0.039Vp - 7.567 \quad (2)$$

The empirical method based on the prediction of the RQD index from Vp values offers an easy way of estimating the mechanical properties of rock masses. However, the result could be integrated with other statistical methods for additional clues. Hence, Table 3 shows the SLR results used as supplementary statistical methods to provide further information on the RMQ of near-surface granitic rock masses in the study area. The estimated RQD and Vp values were regressed as dependent and independent (i.e., predictor) variables, respectively, for the critical

**Table 2**
A comprehensive interpretation of the regression plot to determine the study area's RMQ of near-surface rock masses.

| Class | RMQ | Vp (m/s) | RQD Index (%) | Adjusted rippability |
|---|---|---|---|---|
| I | Excellent | >2100 | >90 | Non-rippable |
| II | Good | 1900–2100 | >75–90 | Marginal |
| III | Fair | 1500–1890 | >50–75 | |
| IV | Poor | 950–1450 | 25–50 | |
| V | Very Poor | 800–940 | <25 | |
| VI | Residual soil | <800 | | Rippable |

**Table 3**
A comprehensive statistical summary of estimated SLR for evaluating RMQ of the near-surface lithologic units in the study area.

| Model summary | | | | | |
|---|---|---|---|---|---|
| Model | R | $R^2$ | Adjusted $R^2$ | Std. Error | Durbin-Watson (D-W) |
| 1 | 0.979 | 0.958 | 0.957 | 5.682 | 1.698 |

| Coefficient | | | | | | | | | | |
|---|---|---|---|---|---|---|---|---|---|---|
| Model | | Unstandardized B | Coefficient Std. Error | Standardized Coefficient (β) | T Stat | *p*-value | 95% Confidence Interval for B | | Collinearity Statistics | |
| | | | | | | | Lower Bound | Upper Bound | Tolerance | VIF |
| 1 | Constant | −7.567 | 2.482 | | −3.049 | 0.004 | −12.57 | −2.564 | | |
| | Vp | 0.039 | 0.001 | 0.979 | 31.708 | <0.0001 | 0.037 | 0.042 | 1.000 | 1.000 |

| ANOVA | | | | | | |
|---|---|---|---|---|---|---|
| Model | | Sum of Square | df | Mean Square | F Stat | *p*-value |
| 1 | Regression | 32458.979 | 1 | 32458.979 | 1005.418 | <0.0001 |
| | Residual | 1420.499 | 44 | 32.284 | | |
| | Total | 33879.478 | 45 | | | |

Dependent variable: RQD
Predictors: (Constant), Vp

evaluation of the SLR model to affirm the statistical significance of the employed variables and the results of the empirical relationship presented in Fig. 9 and Eq. 2.

The parameter R measured the linear correlation strength between RQD and Vp values for rock masses beneath the study area. As presented in Table 3, R had a value of 0.979, suggesting a robust correlation between both used variables (Carroll and Green, 1997; Salkind, 2007). On the other hand, $R^2$ yielded an approximate value of 0.958 (corresponding perfectly to the empirical value generated in Fig. 9), with an adjusted value of 0.957 and a standard error of 5.682. The negligible difference between the estimated $R^2$ and adjust $R^2$ values, with low standard error, affirmed that the model fits reasonably well with the variables; thus, suggesting 95.8% accuracy for the predicted RQD values for the study area. The D-W parameter in statistics is a test to detect the presence of autocorrelation in the residuals from a regression analysis. The D-W value ranges between 0 and 4; a value of 2 means no autocorrelation, values from 0 to <2 indicate positive autocorrelation, and values from 2 to 4 indicate negative autocorrelation (King and Harris, 1995; Kenton, 2021). The D-W test for this study yielded a value of 1.698, suggesting a positive autocorrelation between the used variables (RQD and Vp). As a general rule, D-W values in the range of 1.5 to 2.5 are considered normal, i.e., no autocorrelation between investigated parameters, as Balarabe and Bery (2021) and Akingboye and Bery (2022) explained. Any D-W values <1 or > 3 could cause issues in regression analysis (Field, 2009).

The unstandardized coefficients *B* are the coefficients of the estimated model. Parameter *B* for the statistical model yielded a constant value of −7.567 and a value of 0.039 as the coefficient of Vp, with standard errors of 2.482 and 0.001, respectively. The estimated coefficient values correlated perfectly with the derived empirical relationship for RQD and Vp in Fig. 9. The estimated value of 0.979 for $\beta$ suggests a very strong positive correlation regression between the two used variables. The *T*-values with the corresponding *p*-values (significant values) were used to assess the robustness and accuracy of the estimated coefficients (especially *B*) and the independent variable. Also, the combined evaluation of the *p*-values and the 95% lower and upper confidence intervals are essential parameters to determine the accuracy of statistical analysis. For this study, the regression analysis yielded a *p*-value<0.05% (Table 3), suggesting that the derived values for all analyzed parameters were accurate. In addition, the 95% confidence interval values between 0.013% and 0.017% cover the undetermined RQD values for the study area (Yilmaz and Yuksek, 2009; Freund et al., 2010; González et al., 2019).

On the other hand, ANOVA separated the observed variance data into different components to use as additional tests to determine the relationship between the dependent (RQD) and independent (Vp) variables. The F stat (1005.418) is large, while the *p*-value<0.05% is small. This implies that the independent variable (Vp) has greater explanatory power than expected by chance (Balarabe and Bery, 2021); hence, the results are significant. The results of the F stat influenced the predicted RQD index at a 95% confidence interval level and for a *p*-value<0.0001%, indicating that the model is highly significant (e.g., González et al., 2019; Balarabe and Bery, 2021). The normal P-P plot of

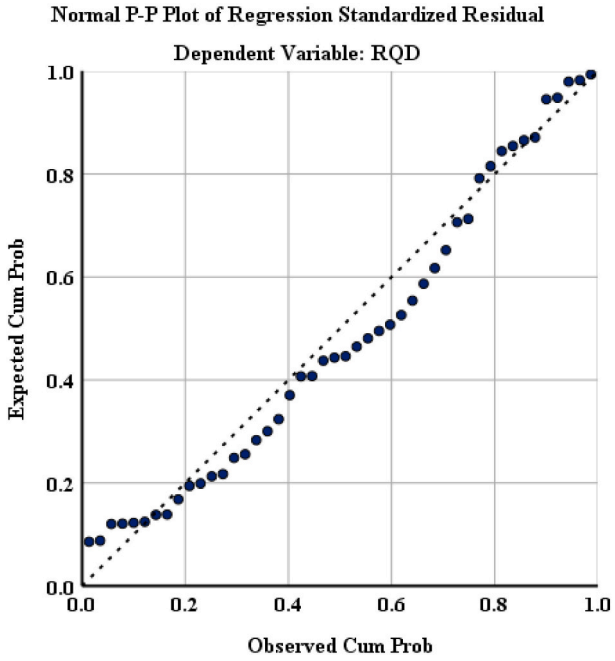


**Fig. 10.** The normal P-P plot of regression standardized residual (stepwise linear regression) for the study area. The dependent variable is RQD against observed cumulative probability on the x-axis and expected cumulative probability on the y-axis.

regression standardized residual (Fig. 10) presents the test of stepwise linear regression for the normality test of the model. The plot displays a generally linear pattern, indicating that the assumption of the model's linearity was not violated, and thus the residuals are normally distributed. The collinearity tolerance value of 1.0 (Table 3) validated the linearity values and suggested that the model was free of collinearity problems (Rugar et al., 2010). Hence, the assumption of homoscedasticity was met in Fig. 10 because the residuals (the difference between the obtained independent (Vp) and the predicted dependent (RQD) variables) and the variance of the residuals were the same for all predicted values, as explained by Tabachnick and Fidell (2007). The scatterplot (Fig. 11) shows no clustering or systematic pattern for the analyzed variables; thus, the assumption of homoscedasticity was also met.

### 4.3. Implications on infrastructure and groundwater development

The impact assessment of the delineated near-surface granitic rock masses beneath the surveyed site on proposed buildings and sustainable groundwater development in the study area is essential to forestall unexpected building collapses and groundwater deficits. Considering the nature and thicknesses of the delineated lithologic units and their rippability conditions, as shown in Figs. 6 and 7, the near-surface rock masses may not support the foundations of superstructures without proper reinforcements. The near-surface crustal architecture exhibited low load-bearing velocity and resistivity characteristics for the residual soil and weathered granitic rock masses, with values ranging from 200 to 1900 m/s and 100–1000 Ω-m, respectively. The evidence of multiple penetrative fractures and water saturation fills within the weathered troughs compounded the above problem (Figs. 6–8). In addition, the rippable residual soils and poor-to-fair granitic rock masses, with values ranging from <800 to <1900 m/s, did not meet the RMQ ratings for the construction of superstructures because Malaysia is one of the leading countries with skyscrapers, particularly in Kuala Lumpur and the Penang States. Besides, the irregular upper bedrock topography and the steep slopes in the northern section of the study area (Fig. 8) may pose severe threats to the foundations of intended buildings.

Nevertheless, the non-ripple fresh granitic bedrocks fulfilled the RMQ ratings for infrastructure designs (e.g., Caterpillar Incorporation, 2010; Griffith and King, 2011; Abzalov, 2016; Ismail et al., 2017). These particular rock masses are Class I rated, with velocity and RQD values of >2100 m/s and >90–100%, respectively (Fig. 9 and Table 2), with the absence of structural features for water retention. Hence, the load of buildings should be transmitted to the non-rippable fresh bedrocks to avert foundation-associated problems like soil sliding, soil liquefaction, and differential settlement. Also, buildings with continuous footing foundations should be found to rest conformably on them. Massive stable non-rippable fresh granitic bedrocks outcropping to the near-surface underpin the area from the central to the northcentral parts; thus, they are suggested as potential zones for building placement. The good-rated granitic rock masses in Class II, with Vp values between 1900 m/s and 2100 m/s and RQD index values of 75% to 90%, may also be considered for the placement of buildings but with reinforced foundations. Rock masses with RQD index values of about >50–75% (fair granitic rock masses) may be considered for shallow-foundation buildings, such as bungalows. Still, the residual soils should be excavated entirely. Preferably, in general, proposed buildings must be piled to the non-rippable bedrocks to rest conformably on the stable/fresh granitic bedrocks in the central and northcentral sections of the surveyed site.

The groundwater potential of the study area, on the other hand, was assessed based on the degree and depths of fractured and weathered zones, as well as the nature of the residual soils and weathered bedrock materials (Christensen et al., 2020). In general, the combined thickness of the residual soils and very poor-to-good granitic layer in the study area is >30 m, including fractured zones and deep-weathered troughs (Figs. 6 and 7). Based on the results of the 3D idealized Vp and rippability models (Fig. 8a–b) and the resistivity models (Fig. 7a–b), the fractured zones beneath Line 1 and towards the central part of Lines 3 and 4 may provide the required groundwater for the proposed buildings in the study area. The identified sections beneath Line 1 and towards the central part of Lines 3 and 4, with appreciably thick silty sand overburden, including deep-weathered troughs and fractures of depths >35 m, and resistivity and Vp values of 100–900 Ω-m and <1900 m/s, respectively, are considered as the potentially water-containing zones for sustainable groundwater abstraction in the study area (e.g., Christensen et al., 2020; Akingboye et al., 2020; Lee et al., 2021; Akingboye and Bery, 2021b, 2022). The high hydraulic gradient of the northeastern section of Line 1 is also an added advantage for speedy water distribution when supplied for use in the buildings. The delineated exploitable zones (drill depths) for groundwater development in the study area agreed with the subsurface lithological characterization and groundwater in the eastern part of Penang Island, in the same geologic terrain, as evaluated by Akingboye and Bery (2021b).

## 5. Conclusions

The characteristics and rippability conditions of near-surface lithologic units in Batu Maung, Penang Island, Malaysia, have been critically evaluated to construct new buildings and sustainable groundwater development using combined SRT, ERT, borehole drilling, and geostatistical analyses. Based on this study, the delineated near-surface layers (residual soils and weathered and fresh granitic units) had Vp and resistivity values ranging from 200 to >2100 m/s and 100 to >2000 Ω-m, respectively. The residual soils and weathered granitic units are

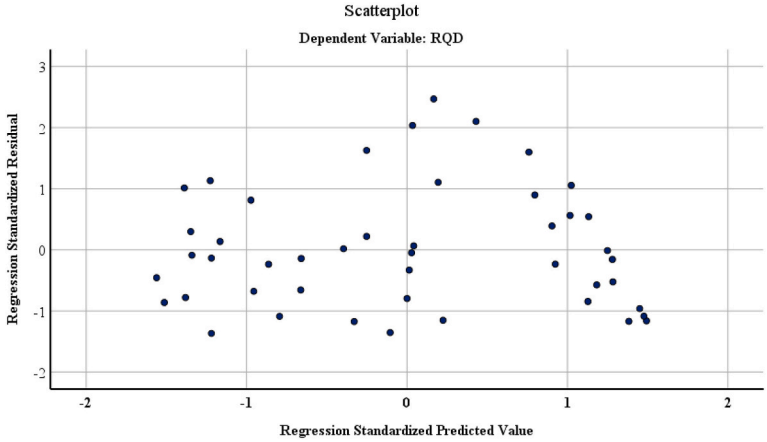


**Fig. 11.** Scatterplot of the regression standardized residual against the regression of standardized predicted value.

silty sand, typically medium and stiff-to-hard. The characteristics of the soils were responsible for the high resistivity values in the uppermost layer of the study area and the fractured and weathered zones. In most sections, fresh granitic units contributed to the observed high velocity and resistivity patterns that interspersed the residual soils. Also, the near-surface geology was characterized by multiple penetrative fractures, especially beneath Lines 3 and 4, starting from the base of the steep slopes to the southeastern parts and western section of the study area. The variabilities of the petrophysical, geomechanical, and structural characteristics of the delineated lithologic units in the area were attributed to the Vp and resistivity values.

Due to the area's structural features and weathering conditions, the delineated near-surface lithologic units were classified based on their rippability conditions from recovered core samples. Based on the observed velocity values, the Vp models identified beneath the study area three categories of lithological units: rippable residual soils, marginal (very poor-to-good) granitic rock masses, and non-rippable granitic rock masses. However, the SLR analysis classified the lithologic units into six classes (i.e., Class I–VI) based on their RMQ derived from RQD and Vp values. The SLR yielded a $R^2$ value of about 95.8% for the predicted empirical relationship between the RQD and Vp parameters. Other SLR analyses yielded the expected results for significantly accurate regressed data, fulfilling all the necessary criteria. As a result, the predicted empirical relationship and RMQ classes for the near-surface granitic rock masses in the study area were precise and can thus be adapted to granitic environments.

Given the nature, thicknesses, and RMQ evaluation of the delineated subsurface crustal architecture of the study area, the near-surface rock masses may not support the foundations of superstructures without proper reinforcements. The RMQ results identified low bearing-load capacities for the residual soils and weathered/fractured granitic units beneath the study area. Hence, all intended buildings, especially high-rise buildings and buildings with continuous footing foundations, should be piled with reinforced concrete foundations to rest on the non-rippable fresh granitic unit, with an RQD of >90% and high-velocity values above 2100 m/s. Massive non-rippable fresh granitic unit outcropping to the near-surface in the central to northcentral parts was identified as potential zones for building placement in the study area. On the contrary, the sustainable groundwater development for the intended buildings in the study area was proposed at sections with thick residual soils and weathered/fractured units with drill depths above 35 m, particularly in the northeastern part of Line 1 and towards the central part of Lines 3 and 4. Overall, the results demonstrated the applicability and efficiency of integrated multi-geotomographic methods and geostatistical analyses to characterize near-surface lithologic units and rock mass rippability and quality in granitic environments.

## CRediT authorship contribution statement

**Adedibu Sunny Akingboye:** Conceptualization, Methodology, Data curation, Software, Formal analysis, Modeling, Validation, Writing – original draft, Writing – review & editing. **Andy Anderson Bery:** Conceptualization, Methodology, Data curation, Software, Formal analysis, Modeling, Validation, Writing – review & editing, Supervision.

## Declaration of Competing Interest

The authors declare that they have no known competing financial interests or personal relationships that could have appeared to influence the work reported in this paper.

## Acknowledgments

We appreciate the comments and suggestions of the Editor-in-Chief and the two anonymous reviewers, which have significantly enhanced the quality and readability of the manuscript. The two undergraduate students and laboratory staff at the Geophysics Unit of School of Physics, Universiti Sains Malaysia, and Messer God'swill Nathan Sambo are also appreciated for their assistance during the field data acquisition.

## References

Abdul Hamid, F.A.Z., Abu Bakar, A.F., Ng, T.F., Ghani, A.A., Mohamad Zulkifley, M.T., 2019. Distribution and contamination assessment of potentially harmful elements (As, Pb, Ni, Cd) in topsoil of Penang Island, Malaysia. Environ. Earth Sci. 78 (21), 616–627.

Abdullah, I., Purwantoa, H.S., 2001. Deformational history of the Eastern Belt, Peninsular Malaysia. Gondwana Res. 4, 556.

Abzalov, M., 2016. Applied Mining Geology. Modern Approaches in Solid Earth Sciences. Springer, p. 448.

Ahmad, F., Yahaya, A.S., Farooqi, M.A., 2006. Characterization and geotechnical properties of Penang residual soils with emphasis on landslides. Amsterd. J. Environ. Sci. 2 (4), 121–128.

Akingboye, A.S., Bery, A.A., 2021a. Performance evaluation of copper and stainless-steel electrodes in electrical tomographic imaging. J. Phys. Sci. 34 (4), 17.

Akingboye, A.S., Bery, A.A., 2021b. Evaluation of lithostratigraphic units and groundwater potential using the resolution capacities of two different electrical tomographic electrodes at dual-spacing. Contrib. Geophys. Geod. 51 (4), 295–320.

Akingboye, A.S., Bery, A.A., 2022. A novel approach to evaluate the nature and rock mass quality of near-surface granitic strata. In: Conference Proceeding of EAGE Middle East Geomechanics Workshop, 1–3 March, Abu Dhabi, UAE, pp. 1–5.

Akingboye, A.S., Ogunyele, A.C., 2019. Insight into seismic refraction and electrical resistivity tomography techniques in subsurface investigations. Rudarsko Geolosko Naftni Zbornik 34 (1), 93–111. https://doi.org/10.17794/rgn.2019.1.9.

Akingboye, A.S., Osazuwa, I.B., 2021. Subsurface geological, hydrogeophysical, and engineering characterization of Etioro-Akoko, southwestern Nigeria, using electrical resistivity tomography. NRIAG J. Astronomy Geophys. 9 (1), 43–57. https://doi.org/10.1080/20909977.2020.1868659.

Akingboye, A.S., Osazuwa, I.B., Mohammed, M.Z., 2020. Electrical resistivity tomography for geo-engineering investigation of subsurface defects: a case study of Etioro-Akoko highway, Ondo State, southwestern Nigeria. Studia Quaternaria 37 (2), 101–107. https://doi.org/10.24425/sq.2020.133754.

Akingboye, A.S., Bery, A.A., Kayode, J.S., Asulewon, A.M., Bello, R., Agbasi, O.E., 2022. Near-surface crustal architecture and geohydrodynamics of the crystalline basement terrain of Araromi, Akungba-Akungba-Akoko, SW Nigeria, derived from multi-geophysical methods. Nat. Resour. Res. 31 (1), 215–236. https://doi.org/10.1007/s11053-021-10000-z.

Alavi, A.H., Sadrossadat, E., 2016. New design equations for estimation of ultimate bearing capacity of shallow foundations resting on rock masses. Geosci. Front. 7, 91–99. https://doi.org/10.1016/j.gsf.2014.12.005.

Anon, 1987. Specifications and Application Handbook, 10th edition. Komatsu, Akasaka, Minato-ku, Tokyo, Japan.

Anon, 1988. Caterpillar Performance Handbook, 19th edition. Caterpillar, Peoria, IL, USA.

Azwin, I.N., Saad, R., Nordiana, M., 2013. Applying the seismic refraction tomography for site characterization. APCBEE Procedia 5, 227–231.

Bailey, A.D., 1975. Rock types and seismic velocity versus rippability. Highway Geol. Sympos. Proc. 26, 135–142.

Balarabe, B., Bery, A.A., 2021. Modeling of soil shear strength using multiple linear regression (MLR) at Penang, Malaysia. J. Eng. Res. 9 (3), 1–12.

Barton, N., 2007. Rock Quality, Seismic Velocity, Attenuation, and Anisotropy. Taylor & Francis Group, London, UK, p. 756.

Barton, N., Lien, R., Lunde, J., 1974. Engineering classification of jointed rock masses for the design of tunnel support. Rock Mech. 6, 189–236.

Basarir, H., 2002. Development of a New Rippability Assessment Method Based on Specific Energy Concept and Numerical Modelling. PhD thesis. Middle East Technical University, Ankara, Turkey.

Basarir, H., Karpuz, C., Tutluoglu, L., 2008. Specific energy based rippability classification system for coal measure rock. J. Terrramech. 45, 51–62. https://doi.org/10.1016/j.jterra.2008.07.002.

Bery, A.A., 2013. High resolution in seismic refraction tomography for environmental study. Int. J. Geosci. 4, 792–796. https://doi.org/10.4236/ijg.2013.44073.

Bery, A.A., Saad, R., 2012a. Correlation of seismic P-wave velocities with engineering parameters (N value and rock quality) for tropical environmental study. Int. J. Geosci. 3, 749–757. https://doi.org/10.4236/ijg.2012.34075.

Bery, A.A., Saad, R., 2012b. Analysis and imaging subsurface structure via engineering characterizations and integrated geophysical tomography modelling methods. Int. J. Geosci. 3, 93–104. https://doi.org/10.4236/ijg.2012.31011.

Binley, A., Kemna, A., 2005. DC Resistivity and Induced Polarization Methods, p. 30. https://doi.org/10.1007/1-4020-3102-5_5.

Cao, J., Yang, X., Du, G., Li, H., 2020. Genesis and tectonic setting of the Malaysian Waterfall granites and tin deposit: constraints from LA–ICP (MC)-MS zircon U–Pb and cassiterite dating and Sr-Nd-Hf isotopes. Ore Geol. Rev. 118, 103336 https://doi.org/10.1016/j.oregeorev.2020.103336.

Carroll, D.J., Green, P.E., 1997. Mathematical Tools for Applied Multivariate Analysis. Elsevier Inc., p. 379. https://doi.org/10.1016/B978-0-12-160954-2.X5000-8

Caterpillar Incorporation, 2010. Caterpillar Performance Handbook, 40th eds. Caterpillar Tractor Company Peoria, Illinois, p. 32. www.CAT.com.

Cheng, Q., Tao, M., Chen, X., Binley, A., 2019. Evaluation of electrical resistivity tomography (ERT) for mapping the soil–rock interface in karstic environments. Environ. Earth Sci. 78, 439. https://doi.org/10.1007/s12665-019-8440-8.

Christensen, C.W., Hayashi, M., Bentley, L.R., 2020. Hydrogeological characterization of an alpine aquifer system in the Canadian Rocky Mountains. Hydrogeol. J. 20. https://doi.org/10.1007/s10040-020-02153-7.

Deere, D.U., 1989. Rock quality designation (RQD) after 20 years. In: U.S. Army Corps of Engineers Contract Report GL-89-1. Waterways Experimental Station, Vicksburg, MS.

Del Potro, R., Hürlimann, M., 2009. A comparison of different indirect techniques to evaluate volcanic intact rock strength. Rock Mech. Rock. Eng. 42, 931–938.

El-Naqa, A., 1996. Assessment of geotechnical characterization of a rock mass using a seismic geophysical technique. Geotech. Geol. Eng. 14 (4), 291–305.

Field, 2009. Autocorrelation Statistical Value of the Durbin-Watson, pp. 220–221.

Freund, R.J., Wilson, W.J., Mohr, D.L., 2010. Statistical Methods, 3rd ed. Elsevier Inc., p. 796. https://doi.org/10.1016/C2009-0-20216-9

Ganerød, G.V., Rønning, J.S., Dalsegg, E., Elvebakk, H., Holmøy, K., Nilsen, B., Braathen, A., 2006. Comparison of geophysical methods for sub-surface mapping of faults and fracture zones in a section of the Viggja road tunnel. *Norway*. Bull. Eng. Geol. Environ. 65, 231–243. https://doi.org/10.1007/s10064-006-0041-6.

González, J., Saldaña, M., Arzúa, J., 2019. Statistical model for predicting the UCS from P-wave velocity, density, and porosity on saturated limestone. Appl. Sci. 9, 5265. https://doi.org/10.3390/app9235265.

Griffith, D.H., King, R.F., 2011. Geomechanical Properties. Physical properties of rocks, In, pp. 245–271.

Hasan, M., Shang, Y., Meng, H., Shao, Yi, X., 2021. Application of electrical resistivity tomography (ERT) for rock mass quality evaluation. Sci. Rep. 11 (1), 23683. https://doi.org/10.1038/s41598-021-03217-8.

Hassan, K., 1990. A summary of the Quaternary geology investigations in Seberang Prai, Pulau Pinang and Kuala Kurau. Bull. Geol. Soc. Malaysia 47–53. https://doi.org/10.7186/bgsm26199005.

Hazreek, Z.A.M., Nizam, Z.M., Aziman, M., Md Dan, M.F., Shaylinda, M.Z.N., Faizal, T.B. M., Aishah, M.A.N., Ambak, K., Rosli, S., Rais, Y., Ashraf, M.I.M., Alel, M.N.A., 2018. Mapping on slope seepage problem using electrical resistivity imaging (ERI). J. Phys. Conf. Ser. 995 (1) https://doi.org/10.1088/1742-6596/995/1/012091.

Hoek, E., Brown, E.T., 1997. Practical estimates of rock mass strength. Int. J. Rock Mech. Min. Sci. 34 (8), 1165–1186.

Hoek, E., Diederichs, M.S., 2006. Empirical estimation of rock mass modulus. Int. J. Rock Mech. Min. Sci. 43 (2), 203–215.

Hung, Y.C., Chou, H.S., Lin, C.P., 2020. Appraisal of the spatial resolution of 2D electrical resistivity tomography for geotechnical investigation. Appl. Sci. 10, 4394.

Ismail, M.A.M., Kumar, N.S., Abidin, M.H.Z., Madun, A., 2017. Rippability assessment of weathered sedimentary rock mass using seismic refraction methods. IOP Conf. Ser. J. Phys. 995, 012105 https://doi.org/10.1088/1742-6596/995/1/012105.

Jug, J., Stanko, D., Grabar, K., Hrženjak, P., 2020. New approach in the application of seismic methods for assessing surface excavatability of sedimentary rocks. Bull. Eng. Geol. Environ. 17. https://doi.org/10.1007/s10064-020-01802-1.

Kenton, W., 2021. Durbin Watson Statistic Definition. Accessed on the 17th of June 2021 at. https://www.investopedia.com/terms/d/durbin-watson-statistic.asp.

Khamehchiyan, M., Dizadji, M.R., Esmaeili, M., 2014. Application of rock mass index (RMi) to the rock mass excavatability assessment in open face excavations. Geomech. Geoeng. 9 (1), 63–71.

King, M.S., 2009. Recent developments in seismic rock physics. Int. J. Rock Mech. Min. Sci. 46, 1341–1348.

King, M.L., Harris, D.C., 1995. The application of the Durbin-Watson test to the dynamic regression model under normal and non-normal errors. Econ. Rev. 14 (4), 487–510.

Lee, S.C.H., Noh, K.A.M., Zakariah, M.N.A., 2021. High-resolution electrical resistivity tomography and seismic refraction for groundwater exploration in fracture hard rocks: a case study in Kanthan, Perak, Malaysia. J. Asian Earth Sci. 218 https://doi.org/10.1016/J.JSEAES.2021.104880.

Liang, M., Mohamad, E.T., Komoo, I., Ma, C.-K., 2017. Performance evaluation of existing surface excavation assessment methods on weathered sedimentary rock. Bull. Eng. Geol. Environ. 76, 205–218.

Loke, M.H., 2004. Rapid 2D resistivity and IP inversion using the least-square method. Manual for RES2DINV version 3.54, 53.

Loke, M.H., Chambers, J.E., Rucker, D.F., Kuras, O., Wilkinson, P.B., 2013. Recent developments in the direct-current geoelectrical imaging method. J. Appl. Geophys. 95, 135–156.

MacGregor, F., Fell, R., Mostyn, G.R., Hocking, G., McNally, G., 1994. The estimation of rock rippability. Q. J. Eng. Geol. 27, 123–144.

McCann, D.M., Fenning, P.J., 2015. Estimation of rippability and excavation conditions from seismic velocity measurements. In: Eddleston, M., Walthall, S., Cripps, J.C., Culshaw, M.G. (Eds.), Engineering Geology of Construction, Geological Society Engineering Geology Special Publication, vol. 10, pp. 335–343.

Mohamad, E.T., Kassim, A.A., Komoo, I., 2005. An overview of existing rock excavatability. Jurnal Kejuruteraan Awan 17 (2), 46–59.

Ng, S.W.P., Chung, S.L., Robb, L.J., Searle, M.P., Ghani, A.A., Whitehouse, M.J., Oliver, G.J.H., Sone, M., Gardiner, N.J., Roselee, M.H., 2015. Petrogenesis of Malaysian granitoids in the Southeast Asian tin belt: Part 1. Geochemical and Sr-Nd isotopic characteristics. Geol. Soc. Amsterd. Bull. 127, 1209–1237.

Ong, W.S., 1993. The Geology and Engineering Geology of Pulau Pinang. Geological Survey of Malaysia, Map Report.

Pullammanappallil, S.K., Louie, J.N., 1994. A generalized simulated-annealing optimization for inversion of first-arrival times. Bull. Seismol. Soc. Am. 84 (5), 1397–1409.

Quigley, P.T., 2006. Ground Proving Seismic Refraction Tomography (SRT) in Laterally Variable Karstic Limestone Terrain. M.Eng. Thesis. University of Florida, p. 143.

Ronczka, M., Wisén, R., Dahlin, T., 2018. Geophysical pre-investigation for a Stockholm tunnel project: joint inversion and interpretation of geoelectric and seismic refraction data in an urban environment. Near Surf. Geophys. 16, 258–268. https://doi.org/10.3997/1873-0604.2018009.

Rugar, T.O., Ayodo, M.O., Agak, J.O., 2010. Rate of financial return to university schooling among lecturers in two public universities in Kenya. Educ. Res. Rev. 5 (3), 130–148.

Salkind, N.J., 2007. Multiple correlation coefficient. In: Encyclopedia of Measurement and Statistics. https://doi.org/10.4135/9781412952644.n298.

Shahbazi, A., Saeidi, A., Chesnaux, R., 2019. A review of existing methods used to evaluate the hydraulic conductivity of a fractured rock mass. Eng. Geol. https://doi.org/10.1016/j.enggeo.2019.105438.

Sheehan, J.R., Doll, W.E., Mandell, W.A., 2005. An evaluation of methods and available software for seismic refraction tomography analysis. J. Environ. Eng. Geophys. 10 (1), 21–34.

Tabachnick, B.G., Fidell, L.S., 2007. Using Multivariate Statistics, 5th ed. Allyn and Bacon, Boston, MA.

Tate, R.B., Tan, D.N.K., Ng, T.F., 2009. Geological Map of Peninsular Malaysia. In: Hutchison, C.S., Tan, Denis N.K. (Eds.), Geology of Peninsular Malaysia. University of Malaya/Geological Society of Malaysia, Kuala Lumpur, p. 107.

Tawaf, M.K., For, M., Amin, M., Asmani, D., Yusof, M., Nizam, S., 2018. Sandstone rippability assessment based on specific energy relationship with tensile strength and surface hardness. J. Adv. Res. Appl. Sci. Eng. Technol. 1 (1), 25–33.

Tsiambaos, G., Saroglou, H., 2010. Excavatability assessment of rock masses using the Geological Strength Index (GSI). Bull. Eng. Geol. Environ. 69, 13–27. https://doi.org/10.1007/s10064-009-0235-9.

Yilmaz, I., Yuksek, G., 2009. Prediction of the strength and elasticity modulus of gypsum using multiple regression, ANN, and ANFIS models. Int. J. Rock Mech. Min. Sci. 46, 803–810.